A Data-Driven Framework for Sparse Impedance Identification of Power Converters in DC Microgrids

Ali Hosseinipour, Javad Khazaei, and Rick S. Blum
Department of Electrical and Computer Engineering
Lehigh University
Bethlehem PA, USA
Email: alh621@lehigh.edu

***Abstract*—Small-signal impedances of source- and load-side power converters are widely used in different stability analysis criteria developed for microgrids. However, these impedances need to be measured at each operating point of the converter by applying perturbation and system identification techniques, which is computationally expensive and time consuming. To address this challenge, a data-driven impedance estimation framework is proposed in this paper to obtain a sparse parameter-varying (SPV) impedance model for power converters in DC microgrids. To this end, an ℓ_0 regularization problem is formulated and solved by the sequential thresholded least-squares (STLS) algorithm to learn coefficient functions of the parametric impedance model of a converter under test (CUT), constructing the SPV impedance model. The identified SPV impedance model is solely reliant on the available feedback signals from the CUT control system to estimate the real-time small-signal impedance. This obviates the need for frequent perturbation of the system at different operating points for the purpose of online stability monitoring. Simulation case studies for a droop-controlled DC-DC converter demonstrate the effectiveness of the SPV impedance model in highly accurate impedance estimation over the frequency range of interest.**

***Index Terms*—DC microgrid, small-signal impedance, sparse identification, stability monitoring**

I. Introduction

DC distributed power systems have found various use cases in stationary and mobile applications such as shipboard power systems, more electric aircrafts, community microgrids, and data centers [1]. Due to the extensive use of power converters and their strong interaction dynamics, stability monitoring is of great importance to mainatin reliable operation of these systems. Eigenvalue and impedance-based approaches are the two major stability analysis methods employed in DC microgrids [2]. The impedance-based analysis is however more suitable for online stability monitoring since the impedance measurement can be performed in real time, whereas detailed analytical models are required for eigenvalue analysis, which are not often available [3]. Various stability analysis criteria have been developed for DC microgrids using source- and load-side impedance models [4].

Online impedance measurement and estimation methods are mostly based on applying wide- or narrow-band perturbation signals using either existing converters in the system or external sources [5]. Wideband online impedance measurement for stability monitoring of DC shipboard power systems is discussed in [6], [7]. In [8], the equivalent bus impedance of a DC microgrid is estimated using wide-band perturbation to measure the voltage loop gain of the source converter and the input impedance of the source converter. Continuous stability monitoring by measuring the impedance using existing converters and employing the nodal stability analysis method is proposed in [9]. All these methods require performing continuous perturbation and post-processing such as fast Fourier transform (FFT) computation, interpolation, and estimation of the output impedance [10]. To address this issue, an impedance estimation method is proposed in [11], which is based on the measurement of control loop gain using Middlebrook's analog injection technique. However, the small-signal perturbation of the system at each operating point is still required. Moreover, the impedance can only be estimated around its peak frequency.

All the above-mentioned online impedance measurement/estimation methods require continuous perturbation of the system at each operating point due to the small-signal nature of the impedance model to be identified. However, the operating point of a DC microgrid is subject to constant variations as a result of the intermittency of the load power and variable energy resources. Therefore, frequent perturbation of the system at each operating point is a computationally intensive task and not ideal for online stability monitoring purposes where run-time efficiency is of great importance. Some recent studies have tackled the operating point dependency of the impedance models for inverter-based resources [12], [13]. These methods use artificial neural networks to estimate an operating-point dependent impedance model of voltage-sourced converters. However, the main drawback of these methods is the requirement for large amount of data, partially due to the use of frequency as one of the inputs to the artificial neural network.

To address the existing knowledge gaps, this paper proposes a data-driven impedance estimation framework for power converters in DC microgrids. The proposed method tackles the operating point dependency of the small-signal impedance model by deriving a sparse parameter-varying (SPV) parametric impedance model using measured impedance data. The SPV impedance model leverages the locally available voltage and current signals to estimate the small-signal impedance in real time. The SPV impedance model obviates the need for frequent perturbation of the system to measure the impedance, improving the run-time efficiency of impedance identification and alleviating computational needs of online stability monitoring systems. The main contributions of the paper can thus be summarized as:

- Development of a machine-learning-based framework to estimate the parametric impedance model of power converters, enabling accurate and rapid impedance estimation without the need for performing constant pertur-

This research was in part under support from the National Science Foundation under Grant NSF-EPCN 2221784. The authors are with the College of Engineering at Lehigh University, Bethlehem, PA 18015 USA.

bation in DC microgrids.
- Proposing the notion of an SPV impedance model to obtain an operating-point dependent impedance model for power converters in DC microgrids by using a regularization technique that decreases the complexity of an estimated impedance model while achieving a good estimation performance.

The rest of the paper is organized as follows. Section II provides information about the study system and the analytical impedance model of the CUT. In Section III, the data-driven impedance estimation framework is proposed and the SPV impedance model is derived. Several case studies are presented in Section IV to validate the SPV impedance model. Section V concludes the paper.

II. System Description and Analytical Impedance Model

A bidirectional DC-DC converter representing a battery power conversion unit is assumed as the CUT according to Fig. 1. The CUT is connected to a typical multi-bus DC microgrid with meshed topology, which provides more reliability compared to radial microgrids [1]. The CUT is equipped with cascaded voltage and current controllers, i.e., $G_v(s)$ and $G_i(s)$. The voltage reference of the CUT, $v_o^*(t)$, is regulated according to the droop control law by

$$v_o^*(t) = v_{ref} - Z_v i_o(t) \tag{1}$$

in order to enable power sharing within a microgrid, where v_{ref} is the nominal output voltage, Z_v is the droop gain, and $i_o(t)$ is the output current of the CUT.

Leveraging first principles and applying the averaging technique over the switching frequency, the state-space averaged model of the CUT is obtained as

$$\frac{d\bar{i}_L(t)}{dt} = \frac{1}{L}[\bar{v}_{in}(t) - r\bar{i}_L(t) - \bar{v}_o(t) + \bar{d}(t)\bar{v}_o(t)] \tag{2}$$

$$\frac{d\bar{v}_o(t)}{dt} = \frac{1}{C}[\bar{i}_L(t) - \bar{d}(t)\bar{i}_L(t) - \bar{i}_o(t)] \tag{3}$$

where $\bar{i}_L(t)$, $\bar{v}_o(t)$, $\bar{v}_{in}(t)$, $\bar{i}_o(t)$, and $\bar{d}(t)$ are the average inductor current, output voltage, input voltage, output current, and duty cycle, respectively.

For the purpose of control design and small-signal stability analysis, (2) and (3) are linearized assuming a constant input voltage for CUT. This then results in the linear time-invariant representation of Fig. 2. From this figure, the closed-loop output impedance of the CUT can be derived as

$$Z_{ocl}(s) = \frac{-\tilde{v}_o}{\tilde{i}_o}\bigg|_{\tilde{v}_{ref},\tilde{v}_i=0} = \frac{Z_{out}(1 + G_iG_{id}) - A_{io}G_iG_{vd} + Z_vG_vG_iG_{vd}}{1 + G_iG_{id} + G_vG_iG_{vd}} \tag{4}$$

where the parameters with the tilde sign represent small-signal parameters. The open-loop transfer functions describing the power stage of the CUT can be derived as

$$Z_{out}(s) = \frac{Ls + r}{LCs^2 + rCs + (1-D)^2} \tag{5}$$

$$G_{vd}(s) = \frac{-LI_Ls - r_LI_L + V_i}{LCs^2 + rCs + (1-D)^2} \tag{6}$$

$$G_{id}(s) = \frac{CV_os + I_L(1-D)}{LCs^2 + rCs + (1-D)^2} \tag{7}$$

$$A_{io}(s) = \frac{-(1-D)}{LCs^2 + rCs + (1-D)^2} \tag{8}$$

where V_o, I_L, D, and V_i represent steady-state values of the output voltage, inductor current, duty cycle of switch S_1, and the input voltage, respectively.

III. Data-Driven Impedance Estimation Framework

As demonstrated in (4)-(8), the output impedance of the CUT is dependent on its operating point. Therefore, for the purpose of online stability monitoring, it is required to measure the impedance as operating point of the CUT varies. The goal of the proposed data-driven impedance estimation framework in Fig. 3 is to obtain a SPV impedance model so that the closed-loop impedance of the CUT can be estimated in real time using only the steady-state measurements of the inductor current and output voltage. This framework is elaborated in the following.

A. Impedance Data Collection

First, frequency scanning is utilized to collect impedance data at multiple operating points of the CUT. To do so, the system is first initialized at a specific operating point. Then the CUT is excited by a pseudo-random binary sequence (PRBS)-driven current source (i_{inj}) at its output terminals as shown in Fig. 1. The magnitude of the PRBS signal is chosen as $0.05|I_o|$ in order to not perturb the system significantly, but collect rich enough data for identification purposes. Next, the impedance frequency-response data is obtained by performing fast fourier transform (FFT) as $Z_{frd}(s) = \frac{\mathcal{F}[v_o(t)]}{\mathcal{F}[-i_o(t)]}$. In order to derive the parametric representation of the measured impedance, a proper transfer function of four poles and three zeros is fitted to the impedance frequency response data using the MATLAB® function `tfest`, resulting in Z_{meas} for a specific operating point of the CUT.

$$Z_{meas}(s) = \frac{b_3s^3 + b_2s^2 + b_1s + b_0}{s^4 + a_3s^3 + a_2s^2 + a_1s + a_0} \tag{9}$$

The procedure for impedance data collection is repeated for m operating points to collect enough data for the estimation problem discussed in the next section.

B. SPV Impedance Model

From the analytical impedance model of the CUT derived in (4), it is clear that the small-signal impedance is a function of the operating point defined by the (I_L, V_o) pair. It should be noted that D can also be represented as a function of V_o and I_L. Therefore, the SPV impedance model of the CUT can be represented by

$$Z_{SPV}(s) = \frac{f_3(I_L,V_o)s^3 + f_2(I_L,V_o)s^2 + f_1(I_L,V_o)s + f_0(I_L,V_o)}{s^4 + g_3(I_L,V_o)s^3 + g_2(I_L,V_o)s^2 + gf_1(I_L,V_o)s + g_0(I_L,V_o)} \tag{10}$$

Each of the coefficient functions, $f(.)$ and $g(.)$ in (10), can be approximated by a linear combination of monomials of V_o and

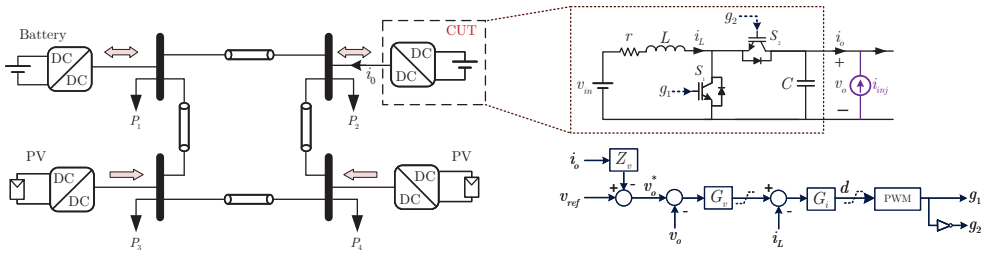

Fig. 1: Circuit and control diagram of the CUT

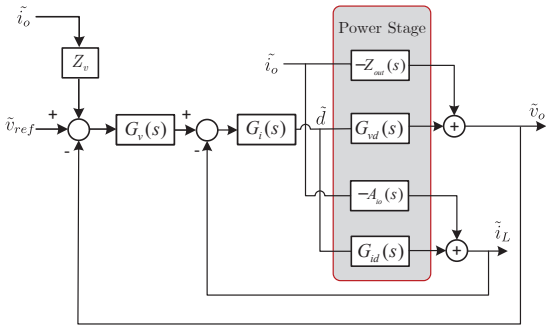

Fig. 2: Small-signal model of the CUT.

I_L. These monomials are identified from a library of candidate functions, $\mathbf{\Theta}$, resulting in sparse coefficient functions. A general guideline to construct the library is to start with low-degree monomials first and introduce more complex functions into the library until a good performance is achieved for the estimation problem. To this end, first the collected impedance data are arranged as $\mathbf{X} = \mathbf{\Theta}(\mathbf{V_o}, \mathbf{I_L})\mathbf{\Xi}$, where $\mathbf{X}$ and $\mathbf{\Theta}$ are given in (11) and (12) with n=8 and p=14.

$$\mathbf{X} = \begin{bmatrix} | & | & | & | & | & | & | & | \\ \mathbf{b_0} & \mathbf{b_1} & \mathbf{b_2} & \mathbf{b_3} & \mathbf{a_0} & \mathbf{a_1} & \mathbf{a_2} & \mathbf{a_3} \\ | & | & | & | & | & | & | & | \end{bmatrix}_{m \times n} \tag{11}$$

The problem of approximating the coefficient matrix $\mathbf{\Xi}$ is then formulated as an ℓ_0 regularization problem of the form

$$\boldsymbol{\xi}_h = \arg\min_{\hat{\boldsymbol{\xi}}_h} ||\mathbf{X}_h - \mathbf{\Theta}(\mathbf{V_o}, \mathbf{I_L})\hat{\boldsymbol{\xi}}_h||_2 + \lambda_h ||\hat{\boldsymbol{\xi}}_h||_0 \tag{13}$$

where $\boldsymbol{\xi}_h$ is the h-th column of $\mathbf{\Xi}$ represented by $\boldsymbol{\xi}_h = \begin{bmatrix} \xi_1 & \xi_2 & \dots & \xi_p \end{bmatrix}^T$. $\mathbf{X}_h$ represents the h-th column of $\mathbf{X}$. The ℓ_2 norm part denoted by $||.||_2$ solves for the least-squares problem. The ℓ_0 norm, $||.||_0$, decides the number of nonzero elements in $\boldsymbol{\xi}_h$, promoting sparsity in the coefficient matrix. λ_h is defined as the regularization factor.

The bi-objective minimization of (13) is solved by the sequential thresholded least squares (STLS) [14], [15]. STLS is an iterative algorithm described by

$$S^k = \left\{ j \in [p] : \left| \xi_j^k \right| \geq \lambda \right\}, \quad k \geq 0 \tag{14}$$

$$\hat{\boldsymbol{\xi}}_h^0 = \mathbf{\Theta}(\mathbf{V_o}, \mathbf{I_L})^\dagger \mathbf{X}_h \tag{15}$$

$$\boldsymbol{\xi}^{k+1} = \underset{\hat{\boldsymbol{\xi}}_h \in \mathbb{R}^p : \mathrm{supp}(\boldsymbol{\xi}_h) \subseteq S^k}{\operatorname{argmin}} \|\mathbf{X}_h - \mathbf{\Theta}(\mathbf{V_o}, \mathbf{I_L})\hat{\boldsymbol{\xi}}_h\|_2, \quad k \geq 0 \tag{16}$$

where k is the iteration number. For an integer $p \in \mathbb{N}$, $[p] := \{1, 2, ..., p\}$. $\mathbf{\Theta}(\mathbf{V_o}, \mathbf{I_L})^\dagger$ is the pseudo-inverse of $\mathbf{\Theta}(\mathbf{V_o}, \mathbf{I_L})$, defined as

$$\mathbf{\Theta}(\mathbf{V_o}, \mathbf{I_L})^\dagger := [\mathbf{\Theta}(\mathbf{V_o}, \mathbf{I_L})^T \mathbf{\Theta}(\mathbf{V_o}, \mathbf{I_L})]^{-1} \mathbf{\Theta}(\mathbf{V_o}, \mathbf{I_L})^T \tag{17}$$

The support set of $\boldsymbol{\xi}_h$ is also defined by $\mathrm{supp}(\boldsymbol{\xi}_h) := \{j \in [p] : \xi_j \neq 0\}$. The psuedocode for the STLS is given in **Algorithm 1**. The algorithm first preforms the least-squares regression to obtain the non-sparse $\hat{\xi}_\mathbf{h}$. The nonsparse $\hat{\xi}_\mathbf{h}$ will include some very small terms, which are then hard thresholded and zeroed out by increasing λ_h. This procedure is repeated for p times, which guarantees the algorithm convergence [15]. The choice of λ_h is crucial in the convergence of the algorithm. While increasing λ_h results in sparser $\xi_\mathbf{h}$, it can lead to an underfit model. On the other hand, small values of λ_h increase the complexity of the model by increasing the number of nonzero coefficients while achieving a smaller error. Therefore, λ_h should be tuned such that a good balance between sparsity and the least-squares error is achieved.

Algorithm 1: STLS Algorithm for Impedance Identification

Data: $\boldsymbol{X}_h$, $\mathbf{\Theta}(\boldsymbol{V_o}, \boldsymbol{I_L})$, λ_h
Result: $\mathbf{\Xi}$
$p \leftarrow 14$;
$n \leftarrow 8$;
for $h = 1 : n$ **do**
  $\hat{\boldsymbol{\xi}}_h^0 = \mathbf{\Theta}^{-1}\mathbf{X_h}$;
  for k = 1 : p **do**
    $\boldsymbol{I}_{small} \leftarrow |\hat{\boldsymbol{\xi}}_h| < \lambda_h$;
    $\boldsymbol{\xi}_h^k(\boldsymbol{I}_{small}) \leftarrow 0$;
    for *all variables* **do**
      $\boldsymbol{I}_{big} \leftarrow\sim \boldsymbol{I}_{small}(:, ii)$;
      $\boldsymbol{\xi}_h(\boldsymbol{I}_{big}, ii) = \mathbf{\Theta}(:, \boldsymbol{I}_{big})^\dagger \mathbf{X_h}(:, ii)$
    end
  end
end

IV. Case Studies

The DC microgrid of Fig. 1 is implemented in Simulink® using the Simscape™ library. The parameters of the CUT are given in Table I. The DC bus nominal voltage is 380 V, which is a standard level in many DC applications [1]. The L and C values are designed so that current and voltage ripples are minimized. $G_v(s)$ and $G_i(s)$ are also designed to ensure zero tracking error well as high stability margins using the Bode plot method. Details on circuit and controller parameters design can be found in [16]. The droop gain, Z_v, is chosen such that the voltage variation of the DC bus is within the 5% of the

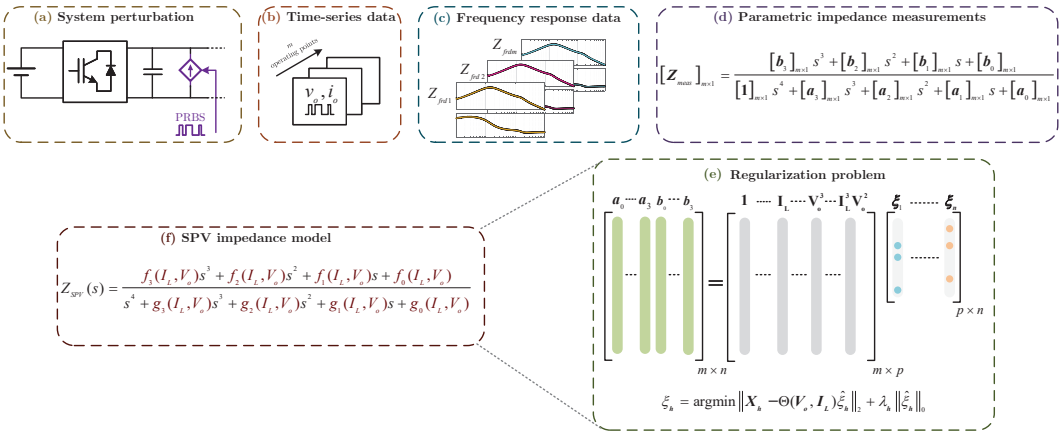

Fig. 3: Data-driven impedance estimation framework to obtain SPV impedance model

$$\boldsymbol{\Theta}(\mathbf{V_o}, \mathbf{I_L}) = \begin{bmatrix} | & | & | & | & | & | & | & | & | & | & | & | & | & | & | \\ \mathbf{1} & \mathbf{V_o} & \mathbf{I_L} & \mathbf{V_o I_L} & \mathbf{V_o^2} & \mathbf{I_L^2} & \mathbf{V_o^2 I_L} & \mathbf{I_L^2 V_o} & \mathbf{V_o^3} & \mathbf{I_L^3} & \mathbf{V_o^3 I_L} & \mathbf{V_o^3 I_L^2} & \mathbf{I_L^3 V_o} & \mathbf{I_L^3 V_o^2} \\ | & | & | & | & | & | & | & | & | & | & | & | & | & | \end{bmatrix}_{m \times p} \tag{12}$$

TABLE I: Simulation parameters of the CUT.

Parameter	Value
v_{in}	250 V
v_{ref}	380 V
L	2.7 mH
C	18.953 μF
r	0.1 Ω
Z_v	3.45
$G_v(s)$	0.0339+25.4/s
$G_i(s)$	0.0723+527/s
Switching frequerncy	20 kHz

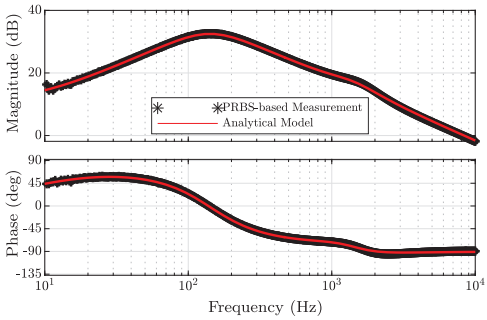

Fig. 4: Measured and analytical impedance model of the CUT (V_o=376.2 V, I_L=1.6 A)

nominal voltage [17]. Following the proposed framework, the impedance data are collected by perturbing the CUT at 90 different operating points ($m = 90$). In order to validate the data collection procedure, the measured impedance is compared with its analytical counterpart in Fig. 4 for a specific operating point. It can be seen that these two impedance models closely match, providing certainty about the validity of the collected data.

A. Regularization factor tuning

The collected data is split such that 65 of them are randomly selected for training and the remaining 25 data points are

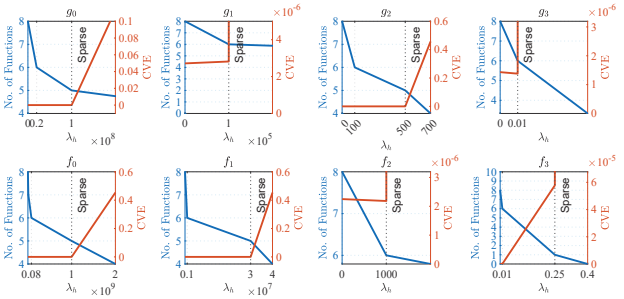

Fig. 5: Derivation of sparse coefficient functions by tuning λ_h

assigned to the testing set. Fig. 5 shows the process of training and testing to obtain the SPV impedance model. In order to estimate the sparse coefficient functions in (10), λ_h is gradually increased from zero (the least-squares solution) until the sparsity is realized for each coefficient function. It can be seen that at the sparse point, all the estimated coefficient functions have fewer active functions from the library $\boldsymbol{\Theta}$ than they have when λ_h=0. Since after the sparse points the cross-validation error (CVE) substantially increases, these points can be considered as the balance between the least-squares error and complexity of the coefficient functions that construct the SPV impedance model. The CVE calculation is performed on the testing set by

$$CVE = \frac{\|\mathbf{X}_{test} - \boldsymbol{\Theta}_{test}(\mathbf{V_o}, \mathbf{I_L})\boldsymbol{\xi}_h\|_2}{\|\mathbf{X}_{test}\|_2} \tag{18}$$

The results of the estimation are given in Table II.

B. SPV Impedance Model Validation

The SPV impedance constructed using the estimated coefficient functions in Table II is compared with the measured impedance model in Fig. 6 at a specific operating point of the CUT that is selected from the testing set. Fig. 6 shows that

TABLE II: Coefficient functions of the SPV impedance model.

Coefficient functions	V_o^2	$V_o^2 I_L$	$I_L^2 V_o$	V_o^3	$V_o^3 I_L$	$I_L^3 V_o$
$g_0(I_L, V_o)$	4.68×10^{8}	3.40×10^{12}	-7.72×10^{12}	0	-8.95×10^{9}	3.10×10^{9}
$g_1(I_L, V_o)$	-2.27×10^{9}	4.81×10^{9}	-1.08×10^{10}	5.98×10^{6}	-1.26×10^{7}	4.59×10^{6}
$g_2(I_L, V_o)$	660.60	4.83×10^{6}	-1.09×10^{7}	0	-1.27×10^{4}	4.40×10^{3}
$g_3(I_L, V_o)$	-339.65	637.68	-1.43×10^{3}	0.89	-1.67	0.61
$f_0(I_L, V_o)$	1.60×10^{9}	2.07×10^{13}	-4.72×10^{13}	0	-5.47×10^{10}	1.90×10^{10}
$f_1(I_L, V_o)$	3.04×10^{7}	2.22×10^{11}	-5.05×10^{11}	0	-5.85×10^{8}	2.02×10^{8}
$f_2(I_L, V_o)$	-1.69×10^{7}	3.82×10^{7}	-8.63×10^{7}	4.47×10^{4}	-1×10^{5}	3.64×10^{4}
$f_3(I_L, V_o)$	0.38	0	0	0	0	0

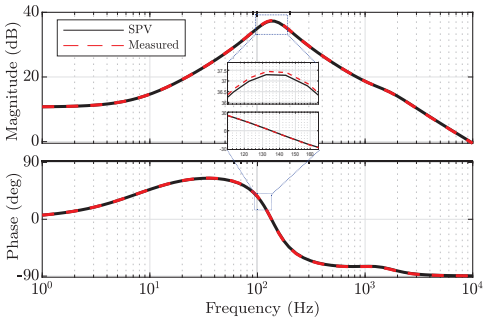

Fig. 6: Validation of the SPV impedance model against its measured counterpart (V_o=391.28 V, I_L=-3.27 A)

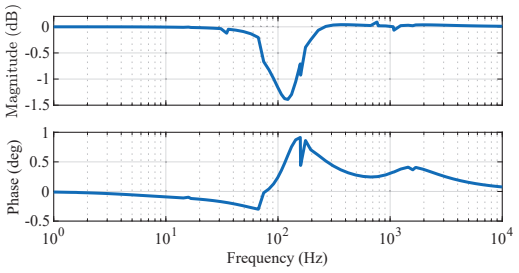

Fig. 7: Error between the SPV impedance model and its measured counterpart (V_o=391.28 V, I_L=-3.27 A)

the SPV impedance model closely conforms to its measured counterpart over the entire frequency range. To further verify the accuracy of the SPV impedance model, the error between the SPV impedance model and its measured counterpart is depicted in Fig. 7. The estimation error is at its highest around the peak frequency, which is still negligible at 1.4 dB for the magnitude and 0.9 deg for the phase.

V. Conclusion

Due to being linear in nature, small-signal impedances of power converters are required to be measured at each operating point of the system in order to perform online stability monitoring in DC microgrids. This paper proposes a data-driven impedance estimation framework that obtains a SPV impedance model for a droop-controlled DC-DC converter within a microgrid. The measured impedance data is utilized to obtain the SPV impedance model by formulating a ℓ_0 regularization algorithm solved by a thresholded algorithm. The estimation performance is shown to be highly accurate over the entire frequency range with only negligible error around the peak frequency. The SPV impedance model solely relies on local voltage and current measurements that are available as feedback signals of the CUT. Therefore, the need for constant perturbation at various operating points is prevented, resulting in a faster impedance estimation procedure that is ideal for online stability monitoring in DC microgrids.

References

[1] D. Kumar, F. Zare, and A. Ghosh, "Dc microgrid technology: System architectures, ac grid interfaces, grounding schemes, power quality, communication networks, applications, and standardizations aspects," *IEEE Access*, vol. 5, pp. 12 230–12 256, 2017.

[2] A. Rygg and M. Molinas, "Apparent impedance analysis: A small-signal method for stability analysis of power electronic-based systems," *IEEE J. Emerg. Sel. Top. Power Electron.*, vol. 5, no. 4, pp. 1474–1486, 2017.

[3] S. Shah, P. Koralewicz, V. Gevorgian, H. Liu, and J. Fu, "Impedance methods for analyzing stability impacts of inverter-based resources: Stability analysis tools for modern power systems," *IEEE Electrif. Mag.*, vol. 9, no. 1, pp. 53–65, 2021.

[4] A. Riccobono and E. Santi, "Comprehensive review of stability criteria for dc distribution systems," in *2012 IEEE Energy Conversion Congress and Exposition (ECCE)*, 2012, pp. 3917–3925.

[5] J. Liu, X. Feng, F. Lee, and D. Borojevich, "Stability margin monitoring for dc distributed power systems via perturbation approaches," *IEEE Trans. Power Electron.*, vol. 18, no. 6, pp. 1254–1261, 2003.

[6] J. Siegers, E. Santi, and A. Barkley, "Wide bandwidth system identification of mvdc distribution system by applying perturbations to an existing converter," in *2013 IEEE Electric Ship Technologies Symposium (ESTS)*, 2013, pp. 434–441.

[7] A. Riccobono, M. Cupelli, A. Monti, E. Santi, T. Roinila, H. Abdollahi, S. Arrua, and R. A. Dougal, "Stability of shipboard dc power distribution: Online impedance-based systems methods," *IEEE Electrif. Mag.*, vol. 5, no. 3, pp. 55–67, 2017.

[8] H. Abdollahi, A. Khodamoradi, E. Santi, and P. Mattavelli, "Online bus impedance estimation and stabilization of dc power distribution systems: A method based on source converter loop-gain measurement," in *2020 IEEE Applied Power Electronics Conference and Exposition (APEC)*, 2020, pp. 3371–3378.

[9] R. Hassan, H. Wang, and R. Zane, "Continuous stability monitoring of dc microgrids using controlled injection," in *2019 IEEE Applied Power Electronics Conference and Exposition (APEC)*, 2019, pp. 1357–1364.

[10] A. Khodamoradi, G. Liu, P. Mattavelli, T. Messo, and H. Abedini, "Prbs-based loop gain identification and output impedance shaping in dc microgrid power converters," *Math. Comput. Simul.*, vol. 183, pp. 129–141, 2021.

[11] A. Khodamoradi, H. Abdollahi, E. Santi, and P. Mattavelli, "A loop gain-based technique for online bus impedance estimation and damping in dc microgrids," *IEEE Trans. Power Electron.*, vol. 36, no. 8, pp. 9648–9658, 2021.

[12] M. Zhang, X. Wang, D. Yang, and M. G. Christensen, "Artificial neural network based identification of multi-operating-point impedance model," *IEEE Trans. Power Electron.*, vol. 36, no. 2, pp. 1231–1235, 2021.

[13] M. Zhang, Q. Xu, and X. Wang, "Physics informed neural network based online impedance identification of voltage source converters," *IEEE Trans. Ind. Electron.*, pp. 1–1, 2022.

[14] S. L. Brunton, J. L. Proctor, and J. N. Kutz, "Discovering governing equations from data by sparse identification of nonlinear dynamical systems," *Proceedings of the National Academy of Sciences*, vol. 113, no. 15, pp. 3932–3937, 2016.

[15] L. Zhang and H. Schaeffer, "On the convergence of the sindy algorithm," *Multiscale Model. Simul.*, vol. 17, no. 3, pp. 948–972, 2019.

[16] M. K. Kazimierczuk, *Pulse-width modulated DC-DC power converters*. John Wiley & Sons, 2015.

[17] J. Khazaei and A. Hosseinipour, *Advances in Data-Driven Modeling and Control of Naval Power Systems*. John Wiley Sons, Ltd, 2022, ch. 21, pp. 453–473.